ACS APPLIED MATERIALS & INTERFACES

Research Article

www.acsami.org

Nanosheet-Based Hierarchical $Ni_2(CO_3)(OH)_2$ Microspheres with Weak Crystallinity for High-Performance Supercapacitor

Guoxing Zhu,*[,†,‡] Chunyan Xi,[†] Mengqi Shen,[§] Chunlin Bao,[†] and Jun Zhu[†]

[†]School of Chemistry and Chemical Engineering, Jiangsu University, Zhenjiang, 212013, China

[‡]State Key Laboratory of Coordination Chemistry, Nanjing University, Nanjing, 210093, China

[§]College of Chemistry, Jilin University, Changchun, 130012, China

Supporting Information

ABSTRACT: Three-dimensionally hierarchical oxide/hydroxide materials have recently attracted increasing interest by virtue of their exciting potential in electrochemical energy conversion and storage. Herein, hierarchical $Ni_2(CO_3)(OH)_2$ microspheres assembled from ultrathin nanosheets were successfully synthesized by a one-pot/one-step hydrothermal route. In this method, common nickel salts and urea were selected as raw materials. The influence of urea concentration on the final product was studied. The hierarchical $Ni_2(CO_3)(OH)_2$ microspheres show weak crystallinity and contain crystalline water. It was found that they exhibit excellent rate capacity when used as supercapacitor electrode. Under current density of 0.5 and 10 A/g, the optimized $Ni_2(CO_3)(OH)_2$ electrode with loading density of 5.3 mg/cm^2 exhibited specific capacitances of 1178 and 613 F/g with excellent cycling stability. The excellent electrochemical property is possibly attributed to the intrinsic nature of $Ni_2(CO_3)(OH)_2$, the ultrathin thickness of nanosheet units, and the sufficient space available to interact with the electrolyte. This facile synthesis strategy and the good electrochemical properties indicate that hydroxycarbonates are promising materials for supercapacitor application. This study suggests a large library of materials for potential application in energy storage systems.

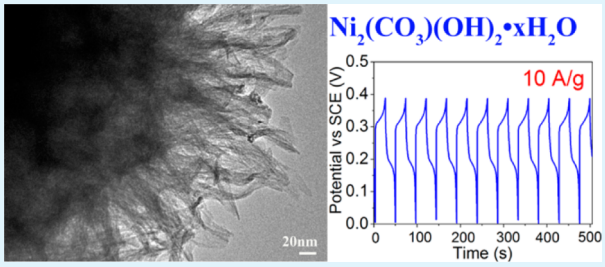

KEYWORDS: *$Ni_2(CO_3)(OH)_2$, nanosheet, hierarchical microsphere, weak crystallinity, supercapacitor, energy storage*

INTRODUCTION

The ever-increasing energy demand and global environmental issues call for not only urgent development of new clean energies but also advanced energy storage and management systems. Supercapacitors with high power density (ca. 5 kW/kg), long lifespan, fast charge and discharge rates, and low maintenance cost are recognized as the most important next-generation energy storage device.[1,2] They demonstrate high potential for offering instantaneous and uninterruptable power for a wide range of devices from portable electronics to new generation hybrid electric vehicles.[3] However, the present typical energy density (<10 Wh/kg) of them is much lower than that of a lithium secondary battery (~200 Wh/kg).[4] The demand, opportunities, and challenges leave room for further exploits.

At the present stage, the hot research is the so-called faradaic pseudocapacitor, which involves electrochemical faradic reactions between electrode materials and ions in electrolyte, thus providing higher energy density. For obtaining a faradaic pseudocapacitor with wonderful performance, suitable electrode materials possessing multiple oxidation states that enable rich redox reactions are desirable.[5] It is preferred that the protons can freely intercalate into its lattice on reduction and out of the lattice on oxidation.[6] In addition, the electrode material should have higher electrochemically accessible surface area but with mediate crystallinity.[7] A well-crystallized structure has difficulty in expanding or contracting, so preventing protons from permeating the bulk material, leading to a diffusion limitation, while amorphous structures would show lower conductivity.

The frequently used electrode materials for faradaic redox pseudocapacitors are transition metal oxides and hydroxides.[8−10] RuO_2 is the most prominent one with specific capacitance as high as 1580 F/g due to its wide potential window, highly reversible redox reactions, and high proton conductivity.[8] However, the commercialization of RuO_2-based electrodes is not promising due to its high cost and the rareness of ruthenium. This inspires the researchers to develop new and low-cost electrode materials with excellent performances. Up to now, some micro/nanostructured materials such as oxides,[11,12] hydroxides,[13,14] sulfides,[15] phosphates,[16−18] and various hybrids[19] have been developed for use in pseudocapacitor with desirable properties. It is affirmed that active materials with hierarchical structures can promote charge transport and ion diffusion, and so improve electrochemical energy storage performances.[20]

Received: July 30, 2014
Accepted: September 12, 2014
Published: September 12, 2014

Hydroxycarbonates with divalent metal ions have the general formula $M_2(CO_3)(OH)_2$, which are widely used materials in industrial processes and are widespread in nature.[21] Recently, there are extensive research efforts devoted to the development of hydroxycarbonates in view of their transformation to porous oxide without structural deformation. For example, $(Cu, Zn)_2(CO_3)(OH)_2$ is in fact the primary phase involved in the production of Cu/ZnO-based catalysts, which are used in methanol synthesis.[22,23] The hydroxycarbonates have unique crystal structures.[24] Most hydroxycarbonates can be described with the similar module, namely, "ribbons" of M^{2+} octahedra, comprising edge-sharing double octahedral chains, that elongate along the *c* axis and interconnect through corner-sharing to form "corrugated" octahedral layers. The connection between adjacent layers is assured by triangular carbonate CO_3^{2-} groups. The hydroxycarbonates also have variable composition, in which the metal ions can be Cu, Zn, Mg, Fe, Co, Ni ion or two of them. The Ni term, nullaginite, $Ni_2(CO_3)(OH)_2$, crystallizes in monoclinic phase ($P2_1/m$),[24] named for the district (in Western Australia) in which it was first found. These hydroxycarbonates may provide a large library of materials for energy storage system.[25]

Herein, we report the facile synthesis of three dimensionally hierarchical dandelion-like $Ni_2(CO_3)(OH)_2{\cdot}xH_2O$ micro/nanostructures and their use as pseudocapacitor electrode. The synthesis is based on a simple one-pot chemical route, that is, heating $Ni(NO_3)_2{\cdot}6H_2O$ and urea in water. The significant features of our synthesis are as follows: (i) The whole process is environmentally friendly and cost-effective without involving any toxic solvents or additives. (ii) The synthesis has high yield and high throughput with gram scale in a 30 mL pot. (iii) The obtained $Ni_2(CO_3)(OH)_2{\cdot}xH_2O$ shows hierarchical structure assembled by ultrathin nanosheets but with weak crystallinity. Excellent pseudocapacitive behaviors are observed for these hierarchical $Ni_2(CO_3)(OH)_2{\cdot}xH_2O$ micro/nanostructures possibly due to the intrinsic nature of this material and their favorable microstructure. The hierarchical $Ni_2(CO_3)(OH)_2{\cdot}xH_2O$ nanostructures based on ultrathin sheetlike units with loading density of 5.3 mg/cm^2 have specific capacitances of 1178.2 and 612.8 F/g at current densities of 0.5 and 10 A/g, respectively. The results indicate that hydroxycarbonates are promising candidate materials for high-performance pseudocapacitor.

EXPERIMENTAL SECTION

Chemicals and Synthesis. All chemicals in this work are of analytical purity and used without further purification. In a typical synthesis, 2.8 g of $Ni(NO_3)_2{\cdot}6H_2O$ was dissolved in 25 mL of distilled water to form a clear solution by magnetic stirring, and then 0.3 g of $CO(NH_2)_2$ was added into the solution. After the solution was stirred for ~10 min, a green solution was obtained. Then, the transparent solution was transferred into a 30 mL Teflon-lined stainless autoclave and heated at 120 °C for 5 h. The solid product of the hydrothermal reaction was washed with distilled water and absolute ethanol several times. The green powder (denoted as HC-0.3) was collected and dried in a vacuum oven at 45 °C for 24 h. For comparison, urea with different amounts (0.1 g, 0.2 g, 0.5 g) was used in controlled experiments, and the samples are denoted as HC-0.1, HC-0.2, HC-0.5, respectively.

Characterization. Crystal phase structures of the synthesized samples were characterized by powder X-ray diffraction (XRD) on a Bruker D-8 Advance diffractometer using Cu Kα (λ = 1.5418 Å) radiation. The morphology and microstructure analyses were conducted on a Hitachi S-4800 field emission scanning electron microscope (FE-SEM) and a JEM-2010 transmission electron microscope (TEM) and high-resolution transmission electron microscope (HRTEM). The Fourier transform infrared (FTIR) spectra were recorded on a Nicolet Nexus 470 FTIR spectrophotometer using a KBr disk. Thermogravimetric differential scanning calorimetry (TG-DSC) analysis is conducted by an integrated thermal analyzer (STA 449C) with a heating speed of 10 °C/min in air.

Electrochemical Test. The cyclic voltammetry investigation was carried out at room temperature on a CHI 760D electrochemical workstation (Shanghai, Chenghua Co.) in a three-electrode system with KOH electrolyte solution (3 M). Cyclic voltammetry experiments were performed at various scan rates of 5, 10, 20, 40, 80 mV/s. The as-prepared $Ni_2(CO_3)(OH)_2{\cdot}xH_2O$ on nickel foam, a platinum foil, and a saturated calomel electrode (SCE) were used as the working electrode, counter electrode, and reference electrode, respectively. For fabricating the working electrode, the as-prepared $Ni_2(CO_3)(OH)_2{\cdot}xH_2O$ material, conductive material (acetylene black), and the binder (polyvinylidene fluoride, PVDF) were mixed in a weight ratio of 80:10:10. The obtained mixture was then coated onto the surface of a piece of nickel foam and then dried at 50 °C under vacuum for 12 h. The mass loading of the active material is carefully weighed on a Beijing sartorius balance (max 120 g; d = 0.1 mg). It was determined to be about 5.3 mg/cm^2. The galvanostatic charge−discharge tests were also performed at room temperature on the CHI 760D electrochemical workstation, in a same three-electrode system with a KOH electrolyte solution (3 M). The galvanostatic charge−discharge tests were performed at various current densities of 0.5, 1, 2, 5, 10 A/g.

RESULTS AND DISCUSSION

The greenish $Ni_2(CO_3)(OH)_2{\cdot}xH_2O$ products were synthesized by the reaction of $Ni(NO_3)_2$ and urea. No any surfactant is involved in the preparation. Figure 1 shows the XRD patterns

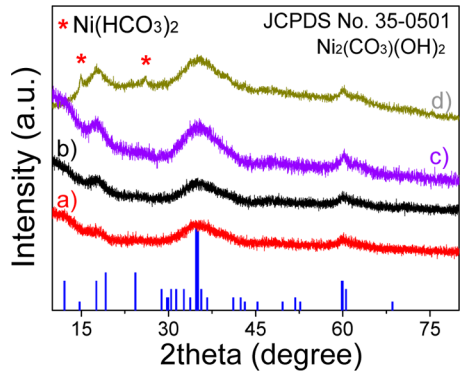

Figure 1. XRD patterns of the product prepared with different urea amounts. (a) 0.1 g, (b) 0.2 g, (c) 0.3 g, and (d) 0.5 g. The relatively sharp peaks in (d) are attributed to the $Ni(HCO_3)_2$ phase. For comparison, the standard pattern of $Ni_2(CO_3)(OH)_2$ (JCPDS No. 35−0501) is shown.

of the products obtained with different urea amounts. The diffraction peaks can be indexed into nullaginite, monoclinic $Ni_2(CO_3)(OH)_2$ (JCPDS Card No. 38−0714), while the pattern shows wide and weak diffraction peaks, suggesting the weak crystallinity, which is favorable for proton permeation when used in supercapacitor electrode.

It was found that the formation of $Ni_2(CO_3)(OH)_2{\cdot}xH_2O$ is urea-amount dependent. If increasing the urea amount to 0.5 g, some relatively sharp diffraction peaks corresponding to $Ni(HCO_3)_2$ are detected, indicating $Ni(HCO_3)_2$ will form with high concentration of urea. Further increasing the urea amount (for example to 1.0 g) will induce the generation of pure $Ni(HCO_3)_2$ phase with high crystallinity.[26] There are some reports that the reaction of transition metal ions and urea

will cause the formation of hydroxycarbonates such as $Cu_2(CO_3)(OH)_2$ and $Zn_2(CO_3)(OH)_2$. The involved reaction can be expressed as follows:

$$CO(NH_2)_2 + H_2O \rightarrow 2NH_3 + CO_2 \quad (1)$$

$$NH_3 + H_2O \rightarrow NH_4^+ + OH^- \quad (2)$$

$$CO_2 + H_2O \rightarrow 2H^+ + CO_3^{2-} \quad (3)$$

$$CO_3^{2-} + CO_2 + H_2O \rightarrow 2HCO_3^- \quad (4)$$

$$CO_3^{2-} + 2OH^- + 2Ni^{2+} \rightarrow Ni_2(CO_3)(OH)_2 \quad (5)$$

$$2HCO_3^- + Ni^{2+} \rightarrow Ni(HCO_3)_2 \quad (6)$$

First, urea is hydrolyzed under heating, forming ammonia and carbon dioxide (reaction 1), which are then transformed into OH^- and CO_3^{2-} (reactions 2 and 3).[27] The combination of OH^-, CO_3^{2-}, and Ni^{2+} induce the formation of $Ni_2(CO_3)(OH)_2$ (reaction 5), while, with higher concentration of $CO(NH_2)_2$, large amounts of CO_2 would form, which will cause the formation of $Ni(HCO_3)_2$ (reactions 4 and 6). In our reaction system, it was found that $Ni_2(CO_3)(OH)_2$ is formed when the urea concentration is below or equal to 0.012 g/mL, while above 0.02 g/mL, the mixture of $Ni_2(OH)_2CO_3$ and $Ni(HCO_3)_2$ or pure $Ni(HCO_3)_2$ is obtained.

Figure 2 shows the SEM images of the prepared $Ni_2(CO_3)(OH)_2{\cdot}xH_2O$ product. Nearly spherical microscale particles are

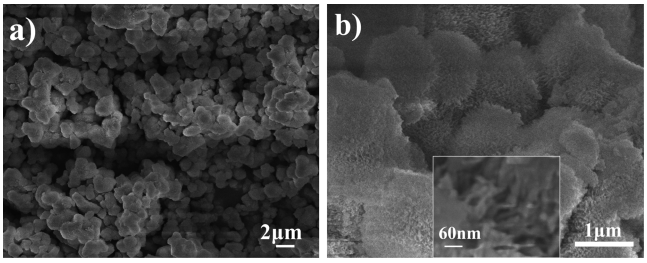

Figure 2. SEM images of the prepared $Ni_2(CO_3)(OH)_2{\cdot}xH_2O$ product (sample HC-0.3) with (a) low and (b) high magnification. (inset) The local magnified surface.

observed. The size locates in the range of 0.8−2.5 μm. From the SEM image with higher resolution, their unique surface microstructure is shown (Figure 2b). It clearly demonstrates the dandelion-like morphology of the $Ni_2(CO_3)(OH)_2{\cdot}xH_2O$ product. Amounts of sheetlike subunits compose into hierarchical dandelion-like microspheres. It was found that the samples obtained with different urea amounts (for the samples HC-0.1, HC-0.2, and HC-0.5) have similar microstructure.

For clearly observing the microstructure, TEM observation was then carried out. As shown in Figure 3, it is evident that bundlelike nanounits assemble into dandelion-like microspheres (Figure 3a,b). This result is consistent with the former SEM observation. There is a strong aggregation trend for the dandelion-like microspheres, inducing the formation of aggregate with size of several micrometers. From TEM images with higher magnification (Figure 3b,c), it is obvious that the bundlelike units are actually sheetlike structures with partial curving. The lower contrast reveals their ultrathin thickness. From the curved position, the thickness of the sheetlike structure is determined to be about 2 nm (as shown by the

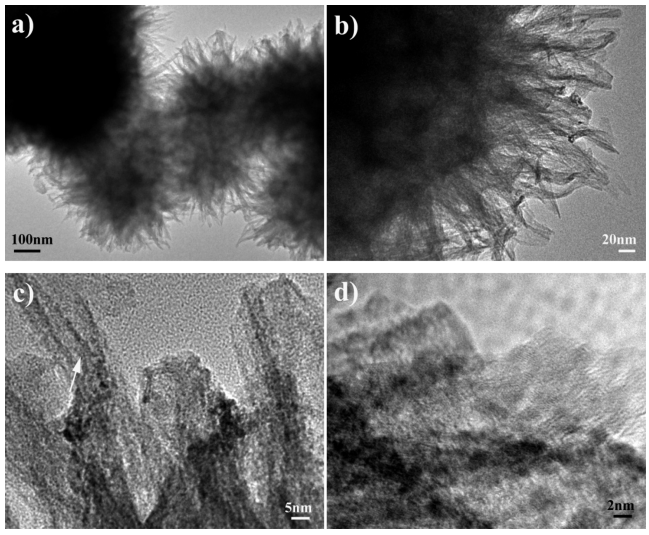

Figure 3. (a, b) TEM and (c, d) HRTEM images of the prepared $Ni_2(CO_3)(OH)_2{\cdot}xH_2O$ product (sample HC-0.3).

arrow in Figure 3c). Moreover, high-resolution TEM (HRTEM) images (Figure 3c,d) illustrate weak lattice fringes, suggesting the weak crystallinity, which is consistent with the XRD result. When used in electrodes, such a unique structure with rich open channels will facilitate the penetration of electrolyte, providing reduced contact resistance and enhanced mass/charge transfer at the electrode/electrolyte interface.[28−30] Moreover, the ultrathin thickness of sheetlike units would shorten the diffusion distance of charges, increase the utilization of active material, and also will be able to accommodate the volume changes during faradaic reaction.[31,32] This feature makes them a promising material for use in energy storage devices or electrodes.

The composition of the synthesized $Ni_2(CO_3)(OH)_2{\cdot}xH_2O$ materials was further investigated by FTIR spectroscopy in the range of 400−4000 cm^{-1}. Figure 4 shows the corresponding IR

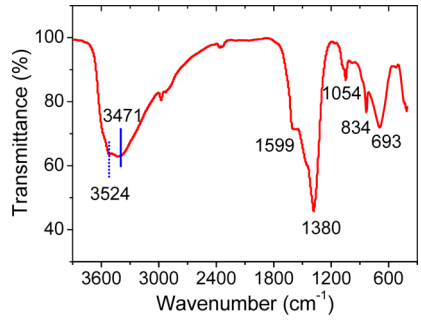

Figure 4. IR spectrum of the prepared $Ni_2(CO_3)(OH)_2{\cdot}xH_2O$ product (sample HC-0.3).

spectrum. The broad band at 3471 cm^{-1} results from hydrogen-bonded O−H groups stretching vibration.[33−35] Two peaks at ~1599 and 3524 cm^{-1} arise from the H−O−H bending vibration and O−H stretching vibration of H_2O, respectively, suggesting the existence of crystal water in the as-synthesized products.[36] The narrow bands at 1380 and 1054 cm^{-1} are ascribed to the asymmetrical and symmetrical stretching vibration modes of CO_3^{2-}, respectively, while the peaks at 693 and 834 cm^{-1} are assigned to in-plane and out-of-plane bending

dx.doi.org/10.1021/am505056d | ACS Appl. Mater. Interfaces 2014, 6, 17208−17214

vibration of CO_3^{2-}. The IR spectrum analysis further confirms the formation of $Ni_2(CO_3)(OH)_2{\cdot}xH_2O$.

$$Ni_2(CO_3)(OH)_2 \rightarrow 2NiO \text{ (calculated weight loss of 29.3\%)} \quad (7)$$

TG analysis ranging from 25 to 1000 °C was conducted in air atmosphere with heating rate of 10 °C/min to investigate its thermal behavior. The corresponding result is shown in Figure 5. The TG curve exhibits two successive decomposing stages,

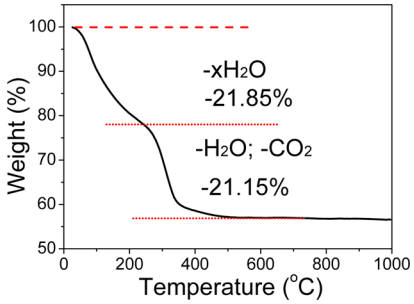

Figure 5. TG analysis of the prepared $Ni_2(CO_3)(OH)_2{\cdot}xH_2O$ product (sample HC-0.3).

corresponding to the dehydration and decarboxylation/dehydration processes, respectively. The first weight loss stage locates at the temperature range of 50−200 °C, the weight loss of about 21.85% can be ascribed to the removal of adsorbed and crystalline water, indicating x in the formula is ∼3. The second mass variation occurs at the temperature range of 250−400 °C, corresponding to a weight loss of 21.15% for the total test sample. For the dehydrated product (namely, the product after the first weight loss step), the weight loss ratio is about 27.1%. This mass loss is related to the decomposition of nickel carbonate hydroxide forming NiO (reaction 7, calculated weight loss of 29.3%). Note that the presence of crystalline water in the product is advantageous for their performance as used in supercapacitance.[37] It is believed that the hydrous regions in materials can allow appreciable protonic conduction, which is critical for high-energy and high-power electrochemical capacitors.

Considering the unique microstructure, weak crystallinity, and the reported good charge storage properties of Ni-based materials such as $Ni(OH)_2$,[38−41] the as-synthesized hierarchical nanosheet-based $Ni_2(CO_3)(OH)_2{\cdot}xH_2O$ product would show excellent properties in charge storage. We first carried out the cyclic voltammetry (CV) measurement in a three-electrode system by using 3 M KOH solution as the electrolyte. The typical CV curves for the hierarchical nanosheet-based $Ni_2(CO_3)(OH)_2{\cdot}xH_2O$ products (samples HC-0.3, HC-0.1) at a scan rate of 20 mV/s are presented in Figure 6a. For comparison, NiO and hierarchical flowerlike $Ni(OH)_2$ products were prepared as our reported method.[26,42] The corresponding CV curves of NiO and hierarchical $Ni(OH)_2$ electrodes are also shown in Figure 6a. It can be clearly observed that both of the tested $Ni_2(CO_3)(OH)_2{\cdot}xH_2O$ electrodes exhibit wider CV curves than NiO and hierarchical $Ni(OH)_2$, demonstrating their higher specific capacitance values.

Figure 6b shows the CV curves for the hierarchical $Ni_2(CO_3)(OH)_2{\cdot}xH_2O$ (HC-0.3) electrode with a series of scan rates (5−80 mV/s) and potential range of 0 to 0.5 V. The CV curves contain one pair of prominent redox peaks. The anodic peak in the potential range of 0.30−0.40 V (vs SCE) is due to the conversion from Ni(II) to Ni(III), while the cathodic peak in the range of 0.08−0.18 V (vs SCE) is attributed to the reverse process. These CV curves show obvious faradic pseudocapacitive features.[43] That is, the capacitance is mainly produced by the redox reactions on the electrode surface. In contrast, for an electric double-layer capacitance, the capacitance is produced by the charge separation at the interface between electrolyte and electrode. The corresponding CV curve is nearly rectangular.[44]

The peak currents increase with the increasing scanning rates, suggesting that this material is beneficial for fast redox reactions. As the scan rate increases, the cathodic and anodic peaks shift in more negative and positive potential as a consequence of the internal resistance of the electrode.[45] The characteristic symmetry of the anodic and cathodic peaks at lower scanning rates suggests the excellent electrochemical reversibility of the nanosheet-based $Ni_2(CO_3)(OH)_2{\cdot}xH_2O$.

According to the following formula, the specific capacitance of the samples can be estimated.

$$C = \frac{1}{m\upsilon(V_c - V_a)} \int_{V_a}^{V_c} I(V)\mathrm{d}V$$

where υ (V/s) is the potential scan rate, m (g) is the active material mass, I (A) is the response current density, and V_a (V) and V_c (V) are the starting and ending potential, respectively. Supporting Information, Figure S1a shows the specific capacitances for various samples with different scanning rates (see Supporting Information). The specific capacitance is negatively correlated with the scan rate, that is, the capacitance decreases with the increasing scan rate. This phenomenon can

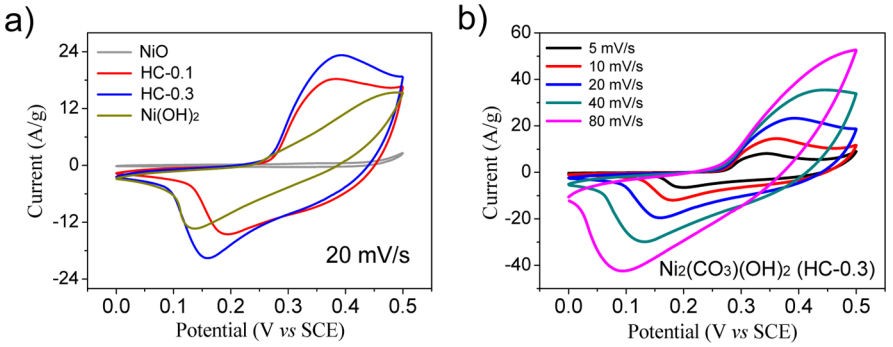

Figure 6. (a) CV curves for different samples under the same scanning rate of 20 mV/s. (b) CV curves for $Ni_2(CO_3)(OH)_2{\cdot}xH_2O$ product (sample HC-0.3) with scanning rates of 5, 10, 20, 40, 80 mV/s.

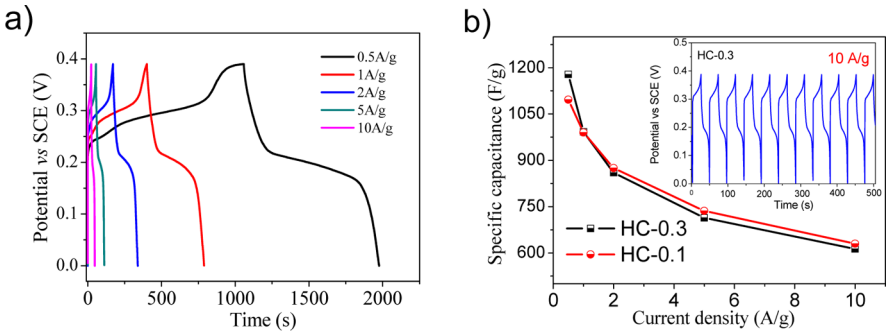

Figure 7. (a) Galvanostatic charge−discharge curves at various current densities (0.5−10 A/g). (b) The corresponding galvanostatic specific capacitors of HC-0.3 and HC-0.1 as a function of the current densities. (inset) The galvanostatic charge/discharge cyclic curves of the first 10 cycles for the HC-0.3 electrode.

be attributed to the full diffusion and migration of electrolytic ions into the active materials at low scan rates. In contrast, with high scan rates, the diffusion effect, limiting the migration of the electrolytic ions, causes some active surface areas to become inaccessible for charge storage.

The loading amount (loading density) also influences the specific capacitance value. With the same loading amount, the specific capacitance of HC-0.3 is a little higher than that of HC-0.1, while the specific capacitance obtained with loading density of 2.65 mg/cm^2 is much higher than that obtained with loading density of 5.3 mg/cm^2 (Figure S1a-i, see Supporting Information). This capacitance difference for two different loading densities exists for various scanning rates. Indeed, it is a common but open question in the test of specific capacitance that a lower loading density induces a high specific capacitance value even for the same sample. This makes the performance comparison of various samples difficult, especially the performance comparison with the literature values, for which sometimes the loading density is not given or much lower for showing a high specific capacitance. A comparison standard is urgently called for specific capacitance test. Note that the loading density of 5.3 mg/cm^2 is used for our study, which is much higher than the usually used density (~1.0 mg/cm^2). If decreasing the loading density, a higher specific capacitance value can be obtained.

Good cycling stability is another important parameter for high-performance supercapacitors. Supporting Information, Figure S1b reveals the cycle performance of the $Ni_2(CO_3)(OH)_2{\cdot}xH_2O$ products (samples HC-0.3, HC-0.1) measured through CV method at a scan rate of 80 mV/s for 1000 cycles (see Supporting Information). After 1000 CV cycles for sample HC-0.3 (Supporting Information, Figure S1b-ii), the specific capacitance is 108% of the initial value, indicating the excellent long-term stability of the nanosheet-based $Ni_2(CO_3)(OH)_2$ electrode. A little increase in specific capacitance during the initial 100 cycles would originate from a possible activation process, allowing the trapped ions to gradually diffuse out.[3] The electrodes fabricated from sample HC-0.1 and sample HC-0.3 with loading density of 2.65 mg/cm^2 also give similar high stability (Supporting Information, Figure S1b-i, S1b-iii). Note that after 500 cycles, the electrodes fabricated from HC-0.3 and HC-0.1 show similar specific capacitor. The good cycling stability would relate to the high structural stability of $Ni_2(CO_3)(OH)_2{\cdot}xH_2O$ electrode during the electrochemical process. After 1000 cycles, the $Ni_2(CO_3)(OH)_2{\cdot}xH_2O$ product was then scraped from the nickel foam substrate for TEM observation. As shown in Figure S2 (see Supporting Information), the unique microstructure, that is, amounts of sheetlike subunits composing into hierarchical dandelion-like microsphere, is kept after the long cycles. This demonstrates the better stability of $Ni_2(CO_3)(OH)_2{\cdot}xH_2O$ product.

To further evaluate the electrochemical properties and estimate the stable potential windows of the as-synthesized $Ni_2(CO_3)(OH)_2{\cdot}xH_2O$ with weak crystallinity, galvanostatic charging and discharging of the same fabricated $Ni_2(CO_3)(OH)_2{\cdot}xH_2O$ electrode (HC-0.3 with loading density of 5.3 mg/cm^2) in 3 M KOH aqueous solution were performed. The charge−discharge curves at different current densities (0.5−10 A/g) between 0.0 and 0.4 V are displayed in Figure 7a. The shape of the discharge curves is representative of pseudocapacitance, which substantiates the CV curve results. The 10 charge−discharge cycles at a current density of 10 A/g (inset, Figure 7b) indicates stable reversible characteristics of the $Ni_2(CO_3)(OH)_2{\cdot}xH_2O$ electrode. The specific capacitance of the electrode can be calculated from the discharge curve according to $C = (I\Delta t/m\Delta V)$ (F/g). Here I is the discharge current (A), Δt is the discharge time (s), m is the mass of the active material in the electrode (g), and ΔV is the potential change during discharge (V). The specific capacitances obtained are 1178.2, 992.3, 859.5, 714.1, and 612.8 F/g at current densities of 0.5, 1, 2, 5, and 10 A/g, respectively (Figure 7b). Considering that the areal capacitance data are more important for supercapacitors at practical level,[11,46,47] the areal capacitance data are calculated based on the working electrode, that is, 6.2, 5.2, 4.5, 3.7, and 3.2 F/cm^2 corresponding to current densities of 0.5, 1, 2, 5, and 10 A/g, respectively. Clearly, the specific capacitance gradually decreases with increasing current density. In the tested current density range, the specific capacitance decreases to 52% of its highest value. The two electrodes of HC-0.3 and HC-0.1 show similar specific capacitance calculated from galvanostatic charging and discharging test, consistent with the results of CV test. These results reveal the relatively high specific capacitance and remarkable rate capability of the hierarchical $Ni_2(CO_3)(OH)_2{\cdot}xH_2O$ nanomaterials for high-performance electrochemical pseudocapacitors.

CONCLUSIONS

In summary, hierarchical nanosheet-based $Ni_2(CO_3)(OH)_2{\cdot}xH_2O$ micro/nanostructures with lower crystallinity have been successfully prepared with urea as precipitant. Ultrathin sheetlike building blocks are self-assembled into hierarchical structures. Lower concentration of urea causes the formation of $Ni_2(CO_3)(OH)_2{\cdot}xH_2O$, while a high concentration of it

induces the generation of $Ni(HCO)_3$. The synthesis with high throughput (grams) and high yield (~100%) is simple without the addition of any organic additives. With the obtained hierarchical nanosheet-based $Ni_2(CO_3)(OH)_2{\cdot}xH_2O$ micro/nanostructures as active electrode materials, a high specific capacity up to 1178 F/g has been achieved with faradaic pseudocapacitance at current density of 0.5 A/g and loading density of 5.3 mg/cm^2. The excellent electrochemical performance with high specific capacitance and long cycle life suggests that hydroxycarbonates are promising materials for pseudocapacitance application. These findings supply new opportunities for hydroxycarbonates and would give some new content for developing high-power energy-storage devices.

■ ASSOCIATED CONTENT

Supporting Information

The specific capacitors calculated from CV curves and the TEM images of the product after long cycles. This material is available free of charge via the Internet at http://pubs.acs.org.

■ AUTHOR INFORMATION

Corresponding Author

*E-mail: zhuguoxing@ujs.edu.cn. Fax: (+86)511-88791800. Phone: (+86)511-88791800.

Notes

The authors declare no competing financial interest.

■ ACKNOWLEDGMENTS

The authors are grateful for financial support from National Natural Science Foundation of China (Grant No. 51102117, 51203069), China Postdoctoral Science Foundation (Grant No. 2012T50439), and Cultivating Project of Young Academic Leader from Jiangsu University.

■ REFERENCES

(1) Dillon, A. C. Carbon Nanotubes for Photoconversion and Electrical Energy Storage. *Chem. Rev.* **2010**, *110*, 6856−6872.

(2) Liu, R.; Duay, J.; Lee, S. B. Redox Exchange Induced MnO_2 Nanoparticle Enrichment in Poly (3,4-ethylenedioxythiophene) Nanowires for Electrochemical Energy Storage. *ACS Nano* **2010**, *4*, 4299−4307.

(3) Simon, P.; Gogotsi, Y. Materials for Electrochemical Capacitors. *Nat. Mater.* **2008**, *7*, 845−854.

(4) Ma, R. Z.; Liu, X. H.; Liang, J. B.; Bando, Y.; Sasaki, T. Molecular-Scale Heteroassembly of Redoxable Hydroxide Nanosheets and Conductive Graphene into Superlattice Composites for High-Performance Supercapacitors. *Adv. Mater.* **2014**, *26*, 4173−4178.

(5) Wang, G. P.; Zhang, L.; Zhang, J. J. Crumpled Nitrogen-Doped Graphene Nanosheets with Ultrahigh Pore Volume for High-Performance Supercapacitor. *Chem. Soc. Rev.* **2012**, *41*, 797−828.

(6) Wu, H. B.; Pang, H.; Lou, X. W. Facile Synthesis of Mesoporous $Ni_{0.3}Co_{2.7}O_4$ Hierarchical Structures for High-performance Supercapacitors. *Energy Environ. Sci.* **2013**, *6*, 3619−3626.

(7) Zheng, J. P.; Cygan, P. J.; Jow, T. R. Hydrous Ruthenium Oxide as an Electrode Material for Electrochemical Capacitors. *J. Electrochem. Soc.* **1995**, *142*, 2699−2703.

(8) Tian, W.; Wang, X.; Zhi, C. Y.; Zhai, T. Y.; Liu, D. Q.; Zhang, C.; Golberg, D.; Bando, Y. $Ni(OH)_2$ Nanosheet@Fe_2O_3 Nanowire Hybrid Composite Arrays for High-performance Supercapacitor Electrodes. *Nano Energy* **2013**, *2*, 754−763.

(9) Jia, Q. X.; Song, S. G.; Wu, X. D.; Cho, J. H.; Foltyn, S. R.; Findikoglu, A. T.; Smith, J. L. Epitaxial Growth of Highly Conductive RuO_2 Thin Films on (100) Si. *Appl. Phys. Lett.* **1996**, *68*, 1069−1071.

(10) Xu, Y. X.; Huang, X. Q.; Lin, Z. Y.; Zhong, X.; Huang, Y.; Duan, X. F. One-step Strategy to Graphene/$Ni(OH)_2$ Composite Hydrogels as Advanced Three-dimensional Supercapacitor Electrode Materials. *Nano Res.* **2013**, *6*, 65−76.

(11) Lu, X. H.; Zeng, Y. X.; Yu, M. H.; Zhai, T.; Liang, C. L.; Xie, S. L.; Balogun, M. S.; Tong, Y. X. Oxygen-Deficient Hematite Nanorods as High-Performance and Novel Negative Electrode for Flexible Asymmetric Supercapacitors. *Adv. Mater.* **2014**, *26*, 3148−3155.

(12) Wang, Q. F.; Wang, X. F.; Xu, J.; Ouyang, X.; Hou, X. J.; Chen, D.; Wang, R. M.; Shen, G. Z. Flexible Coaxial-type Fiber Supercapacitor Based on $NiCo_2O_4$ Nanosheets Electrodes. *Nano Energy* **2014**, *8*, 44−51.

(13) Li, H. B.; Yu, M. H.; Lu, X. H.; Liu, P.; Liang, Y.; Xiao, J.; Tong, Y. X.; Yang, G. W. Amorphous Cobalt Hydroxide with Superior Pseudocapacitive Performance. *ACS Appl. Mater. Interfaces* **2014**, *6*, 745−749.

(14) Dam, D. T.; Lee, J. M. Ultrahigh Pseudocapacitance of Mesoporous Ni-doped $Co(OH)_2$/ITO Nanowires. *Nano Energy* **2013**, *2*, 1186−1196.

(15) Yu, L.; Zhang, L.; Wu, H. B.; Lou, X. W. Shape-Controlled Synthesis of $CoNi_2S_4$ Microstructures from Precursors: A Study of Their Catalytic Application to *p*-Nitrophenol Reduction. *Angew. Chem., Int. Ed.* **2014**, *53*, 3711−3714.

(16) Pang, H.; Wang, S. M.; Shao, W. F.; Zhao, S. S.; Yan, B.; Li, X. R.; Li, S. J.; Chen, J.; Du, W. M. Few-layered $CoHPO_4{\cdot}3H_2O$ Ultrathin Nanosheets for high Performance of Electrode Materials for Supercapacitors. *Nanoscale* **2013**, *5*, 5752−5757.

(17) Wang, S. M.; Pang, H.; Zhao, S. S.; Shao, W. F.; Zhang, N. N.; Zhang, J. S.; Chen, J.; Li, S. J. $NH_4CoPO_4{\cdot}H_2O$ Microbundles Consisting of One-dimensional Layered Microrods for High Performance Supercapacitors. *RSC Adv.* **2014**, *4*, 340−347.

(18) Pang, H.; Wei, C. Z.; Ma, Y. H.; Zhao, S. S.; Li, G. C.; Zhang, J. S.; Chen, J.; Li, S. J. Nickel Phosphite Superstructures Assembled by Nanotubes: Original Application for Effective Electrode Materials of Supercapacitors. *ChemPlusChem* **2013**, *78*, 546−553.

(19) Zhou, D.; Su, X. R.; Boese, M.; Wang, R. M.; Zhang, H. Z. $Ni(OH)_2$@$Co(OH)_2$ Hollow Nanohexagons: Controllable Synthesis, Facet-selected Competitive Growth and Capacitance Property. *Nano Energy* **2014**, *5*, 52−59.

(20) Wei, T. Y.; Chen, C. H.; Chien, H. C.; Lu, S. Y.; Hu, C. C. A Cost-effective Supercapacitor Material of Ultrahigh Specific Capacitances: Spinel Nickel Cobaltite Aerogels from an Epoxid-Driven Sol-gel Process. *Adv. Mater.* **2010**, *22*, 347−351.

(21) Merlini, M.; Perchiazzi, N.; Hanfland, M.; Bossak, A. Phase Transition at High Pressure in $Cu_2(CO_3)(OH)_2$ Related to the Reduction of the Jahn-Teller Effect. *Acta Crystallogr., Sect. B: Struct. Sci.* **2012**, *68*, 266−274.

(22) Behrens, M.; Kasatkin, I.; Kuhl, S.; Weinberg, G. Phase-Pure Cu, Zn, Al Hydrotalcite-like Materials as Precursors for Copper Rich Cu/ZnO/Al_2O_3 Catalysts. *Chem. Mater.* **2010**, *22*, 386−397.

(23) Porta, P.; Rossi, S. D.; Ferraris, G.; Jacono, M. L.; Minelli, G.; Moretti, G. Structural Characterization of Malachite-like Coprecipitated Precursors of Binary CuO-ZnO Catalysts. *J. Catal.* **1988**, *109*, 367−377.

(24) Nickel, E. H.; Berry, L. G. The New Mineral Nullaginit and Addtional Data on the Related Mineral Srosasit and Glaukosphaerite. *Can. Mineral.* **1981**, *19*, 315−324.

(25) Lu, Z. Y.; Zhu, W.; Lei, X. D.; Williams, G. R.; Hare, D. O.; Chang, Z.; Sun, X. M.; Duan, X. High Pseudocapacitive Cobalt Carbonate Hydroxide Films derived from CoAl Layered Double Hydroxides. *Nanoscale* **2012**, *4*, 3640−3643.

(26) Zhu, G. X.; Xi, C. Y.; Xu, H.; Zheng, D.; Liu, Y. J.; Xu, X.; Shen, X. P. Hierarchical NiO Hollow Microspheres Assembled from Nanosheet-stacked Nanoparticles and Their Application in a Gas Sensor. *RSC Adv.* **2012**, *2*, 4236−4241.

(27) Wang, X. B.; Cai, W. P.; Lin, Y. X.; Wang, G. Z.; Liang, C. H. Mass Production of Micro/nanostructured Porous ZnO PPlates and their Strong Structurally Enhanced and Selective Adsorption Performance for Environmental Remediation. *J. Mater. Chem.* **2010**, *20*, 8582−8590.

(28) Beaudrouet, E.; LeGalLaSalle, A.; Guyomard, D. Nanostructured Manganese Dioxides: Synthesis and Properties as Supercapacitor Electrode Materials. *Electrochim. Acta* **2009**, *54*, 1240−1248.
(29) Yan, J.; Wang, Q.; Wei, T.; Fan, Z. Recent Advances in Design and Fabrication of Electrochemical Supercapacitors with High Energy Densities. *Adv. Energy Mater.* **2014**, *4*, 1300816−1−43.
(30) Kim, B. K.; Chabot, V.; Yu, A. P. Carbon Nanomaterials Supported $Ni(OH)_2$/NiO Hybrid Flower Structure for Supercapacitor. *Electrochim. Acta* **2013**, *109*, 370−380.
(31) Hu, C. C.; Chang, K. H.; Lin, M. C.; Wu, Y. T. Design and Tailoring of the Nanotubular Arrayed Architecture of Hydrous RuO_2 for Next Generation Supercapacitors. *Nano Lett.* **2006**, *6*, 2690−2695.
(32) Jiang, J.; Li, Y. Y.; Liu, J. P.; Huang, X. T.; Yuan, C. Z.; Lou, X. W. Recent Advances in Metal Oxide-based Electrode Architecture Design for Electrochemical Energy Storage. *Adv. Mater.* **2012**, *24*, 5166−5180.
(33) Guan, X. Y.; Deng, J. C. Preparation and Electrochemical Performance of Nanoscale Nickel Hydroxide with Different Shapes. *Mater. Lett.* **2007**, *61*, 621−625.
(34) Sun, D. H.; Zhang, J. L.; Ren, H. J.; Cui, Z. F.; Sun, D. X. Influence of OH^- and SO_4^{2-} Anions on Morphologies of the Nanosized Nickel Hydroxide. *J. Phys. Chem. C* **2010**, *114*, 12110−12116.
(35) Ramesh, T. N.; Kamath, P. V. Synthesis of nickel hydroxide: Effect of Precipitation Conditions on Phase Selectivity and Structural Disorder. *J. Power Sources* **2006**, *156*, 655−661.
(36) Zhang, Q. J.; Zhu, G. X.; Shen, X. P.; Tong, L.; Ye, Z. F.; Chen, K. M. Coordination Polymer Micro/nano-crystals: Controlled Synthesis and Formation Mechanism in the Case of $Mn_2Mo(CN)_8{\cdot}xH_2O$. *CrystEngComm* **2013**, *15*, 2909−2915.
(37) Long, J. W.; Swider, K. E.; Merzbacher, C. I.; Rolison, D. R. Voltammetric Characterization of Ruthenium Oxide-based Aerogels and Other RuO_2 Solids: the Nature of Capacitance in Nanostructured Materials. *Langmuir* **1999**, *15*, 780−785.
(38) Ji, J. Y.; Zhang, L. L.; Ji, H. X.; Li, Y.; Zhao, X.; Bai, X.; Fan, X. B.; Zhang, F. B.; Ruoff, R. S. Nanoporous $Ni(OH)_2$ Thin Film on 3D Ultrathin-Graphite Foam for Asymmetric Supercapacitor. *ACS Nano* **2013**, *7*, 6237−6243.
(39) Wang, H. L.; Casalongue, H. S.; Liang, Y. Y.; Dai, H. J. $Ni(OH)_2$ Nanoplates Grown on Graphene as Advanced Electrochemical Pseudocapacitor Materials. *J. Am. Chem. Soc.* **2010**, *132*, 7472−7277.
(40) Cheng, K.; Yang, F.; Ye, K.; Li, Y. J.; Yang, S. N.; Yin, J. L.; Wang, G. L.; Cao, D. X. Facile Preparation of Transition Metal Oxide-metal Composites with Unique Nanostructures and Their Electrochemical Performance as Energy Storage Material. *J. Mater. Chem. A* **2013**, *1*, 14246−14252.
(41) Wang, Y.; Gai, S. Y.; Niu, N.; He, F.; Yang, P. P. Fabrication and Electrochemical Performance of 3D Hierarchical β-$Ni(OH)_2$ Hollow Microspheres Wrapped in Reduced Graphene Oxide. *J. Mater. Chem. A* **2013**, *1*, 9083−9091.
(42) Zhu, G. X.; Liu, Y. J.; Xi, C. Y.; Bao, C. L.; Xu, H.; Shen, X. P.; Zhu, X. L. Polymer Guided Synthesis of $Ni(OH)_2$ with Hierarchical Structure and their Application as the Precursor for Sensing Materials. *CrystEngComm* **2013**, *15*, 9189−9195.
(43) Yuan, C. Z.; Zhang, X. G.; Su, L. H.; Gao, B.; Shen, L. F. Facile Synthesis and Self-Assembly of Hierarchical Porous NiO Nano/micro Spherical Superstructures for High Performance Supercapacitors. *J. Mater. Chem.* **2009**, *19*, 5772−5777.
(44) Dai, L. M.; Chang, D. W.; Baek, J. B.; Lu, W. Carbon Nanomaterials for Advanced Energy Conversion and Storage. *Small* **2012**, *8*, 1130−1166.
(45) Xu, J.; Dong, Y. Z.; Cao, J. Y.; Guo, B.; Wang, W. C.; Chen, Z. D. Microwave-incorporated Hydrothermal Synthesis of urchin-like $Ni(OH)_2$-$Co(OH)_2$ Hollow Microspheres and their Supercapacitor Applications. *Electrochim. Acta* **2013**, *114*, 76−82.
(46) Zhai, T.; Lu, X. H.; Ling, Y. C.; Yu, M. H.; Wang, G. M.; Liu, T. Y.; Liang, C. L.; Tong, Y. X.; Li, Y. A New Benchmark Capacitance for Supercapacitor Anodes by Mixed-Valence Sulfur-Doped V_6O_{13-x}. *Adv. Mater.* **2014**, *26*, 5869−5875.
(47) Lu, X. H.; Yu, M. H.; Wang, G. M.; Tong, Y. X.; Li, Y. Flexible Solid-State Supercapacitors: Design, Fabrication and Applications. *Energy Environ. Sci.* **2014**, *7*, 2160−2181.